S. Afr. J. mar. Sci. 21: 235–249
1999

A BIOPHYSICAL MODEL APPLIED TO THE BENGUELA UPWELLING SYSTEM

*M. D. SKOGEN**

A three-dimensional biophysical model for the Benguela upwelling system is described. The model (NORWECOM) has been used in previous works to study model circulation, primary production and dispersion of particles (fish larvae and pollution) in the North Sea. The primary task of this work has been to validate its implementation in the Benguela upwelling system by reproducing several of the main characteristics in the area. The results show a well-developed Agulhas Current, the Agulhas retroflection and Agulhas rings. The model is also able to identify main upwelling cells in their correct location, the Angola-Benguela front and a longshore thermal front outside the upwelling area. The Benguela Current and a poleward undercurrent, following the shelf-break, is also shown.

The Benguela system, part of the South-East Atlantic and lying between 14 and 37°S, is one of four major eastern boundary current regions of the world. The oceanography in all these are dominated by a coastal upwelling system. The Benguela is unique in that it is bounded at both the equatorward and poleward ends by warm water. The strong upwelling gives a high primary productivity, which again supports large commercial fisheries. The Benguela ecosystem displays intra-, interannual and decadal variability, and this impacts on its living marine resources. An overview of the principal characteristics of the Benguela, including its overlying wind fields, oceanic boundaries and fronts, deep and shelf circulation and system variability can be found in Shannon and Nelson (1996).

Fish recruitment, growth and distribution is, to a large extent, dependent on changing environmental variables. It is expensive and time consuming to measure these variables and the need for predictive numerical models becomes obvious as a tool for inter- and extrapolation in both space and time of spot measurements at sea. The present paper is meant to be a step towards such a model for the Benguela upwelling system.

Several models, of different complexity and resolution, have been used to study the whole or parts of the Benguela. Among these, Van Foreest and Brundrit (1982) described a linear, two-mode numerical model, which was used to discuss upwelling for a region along the south-western coast of Africa. In a multilayer modelling study of the winddriven South Atlantic/Indian Ocean circulation and Agulhas retroflection region, Boudra and De Ruiter (1986) and Boudra and Chassignet (1988) showed the formation of rings at the retroflection. One of the first large-scale circulation models, including the South-East Atlantic and the Benguela upwelling system, was the FRAM (Fine Resolution Antarctic Model) model (The FRAM Group 1991). In a series of papers, Lutjeharms *et al*. (1991, 1995) and Lutjeharms and Webb (1995) have shown its applicability in the region in question. Holland *et al*. (1991) used satellite altimeter data for assimilation in a regional ocean model of the Agulhas retroflection. Using a simple conceptual model, Fennel (1999) provided a theoretical study of the Benguela system, including coastal jets, upwelling and Kelvin waves.

The present model is the first large-scale model for the Benguela upwelling system in which physical and biological processes are coupled. After a short model description, in which the initial conditions and forcing factors are presented, the results and discussion section is divided into several parts. The first looks at the mean circulation, salinity and temperatures from the model, with the focus on some of the main characteristics for the area. The model's ability to model Agulhas rings is then investigated, and then the results for the primary production are used to identify the upwelling cells. Finally, some concluding remarks and plans for future work are given.

MODEL DESIGN

The NORWegian ECOlogical Model system (NORWECOM) is a coupled physical, chemical, biological model system applied to study primary production and dispersion of particles (fish larvae, pollution). The model is fully described by Skogen (1993) (see also Aksnes *et al*. 1995 and Skogen *et al*. 1995). It has been validated by comparison with field data in the North Sea/Skagerrak and Norwegian Sea (North-East Atlantic) in Svendsen *et al*. (1995, 1996), Berntsen *et al*. (1996) and Skogen *et al*. (1997).

* Institute of Marine Research, Pb 1870 Nordnes, 5817, Bergen, Norway. E-mail: morten@imr.no

Manuscript received: June 1998

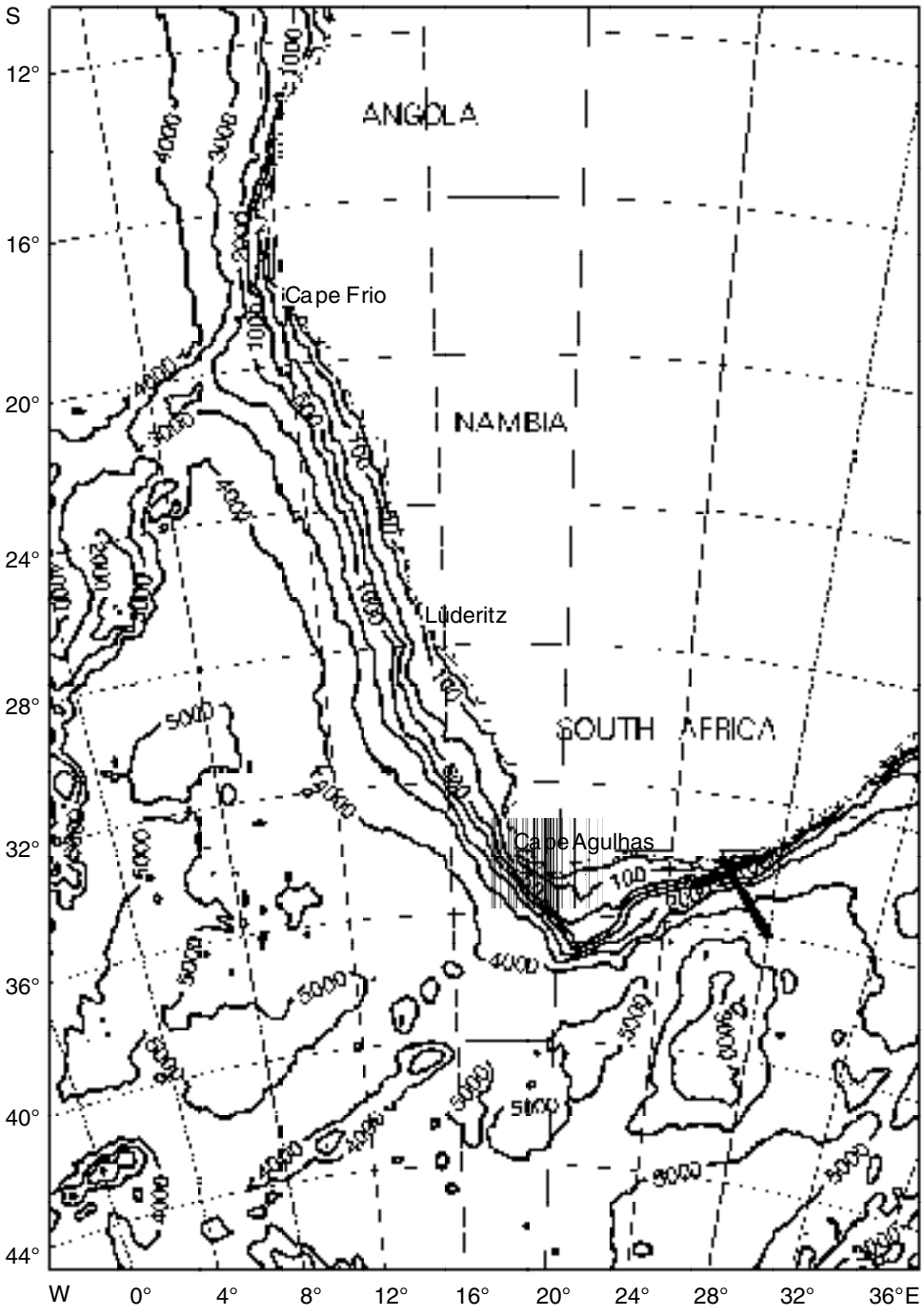

Fig. 1: Model domain showing bottom topography and the Port Elizabeth section

The physical model

The physical model is based on the three-dimensional, primitive equation, time-dependent, wind- and density-driven Princeton Ocean Model (POM, Blumberg and Mellor 1987). The prognostic variables of this model are: three components of the velocity field, temperature, salinity, turbulent kinetic energy, a turbulent macroscale and the water level. The governing equations of the model are the horizontal momentum equations, the hydrostatic approximation, the continuity equation, conservation equations for temperature and salinity, and a turbulence closure model for calculating the two turbulence variables (Mellor and Yamada 1982). The equations and boundary conditions are approximated by finite difference techniques in an Arakawa C-grid (Mesinger and Arakawa 1976).

For the present study, the model is used with a horizontal resolution of 20×20 km, on a grid covering the African coast and the open ocean from about 12 to 46°S and from 4 to 30°E (Fig. 1). The bottom topography is inter-and extrapolated from data from the South African Naval Hydrographic Office and from the General Bathymetric Chart of the Oceans (GEBCO) digital atlas (IOC, IHO and BODC 1994). In the vertical, 18 bottom-following σ layers are used.

The forcing variables are six-hourly hindcast atmospheric pressure fields and 6-hourly wind-stress fields, interpolated from a 1.125×1.125 degree grid from the Meteorological ARchive System (MARS) at the European Centre of Meteorology and Weather Forecast, Reading, UK (ECMWF). Initial values (monthly fields) for salinity and temperature are interpolated from the 1×1 degree NOAA Atlas (Levitus and Boyer 1994, Levitus *et al*. 1994), whereas the initial fields for velocities and water elevation are derived from the density fields, using the thermal wind equation and assuming zero net flux in each water column. Interpolation between these monthly fields are also used at all open boundaries. To absorb inconsistencies between the forced boundary conditions and the model results, a seven gridcell "Flow Relaxation Scheme" (FRS) zone (Martinsen and Engedahl 1987) is used around these open boundaries. In the zone, each prognostic variable (ϕ) is simply updated by the translation $\phi = (1 - \beta)\ \phi_{int} + \beta\phi_{ext}$, where ϕ_{int} contains the time-integrated, unrelaxed values calculated in the entire model domain, i.e. also in the areas covered by the FRS-zone, and ϕ_{ext} is the specified external solution in the zone. ϕ is the new value and β is a relaxation parameter, which varies from 0, at the end of the zone facing the interior model domain, to 1 at the outer end of the zone.

In the lack of appropriate data on the surface heat fluxes, a "relaxation towards climatology" method is used for the surface layer (Cox and Bryan 1984). During calm wind conditions, the surface temperature field will adjust to the climatological values after about 10 days (Oey and Chen 1992). For deep water (below 500 m), a weak relaxation to climatological salinity and temperature fields is performed (Sarmiento and Bryan 1982), so that the model does not drift too far from known values. The time factor in this relaxation increases with depth. The net evaporation precipitation flux is set to zero. At present, freshwater runoff from rivers and tidal forcing are not included in the Benguela implementation.

The biological model

The biological model is coupled to the physical model through the subsurface light field, the hydrography and the horizontal and the vertical movement of the water masses.

The prognostic variables are: inorganic nitrogen, phosphorus and silicate, two different types of phytoplankton (diatoms and flagellates), detritus (dead organic matter), light in the water column, and turbidity. Phytoplankton production is affected by nutrients, surface irradiance, temperature and the attenuation/turbidity of the water. The attenuation coefficient is a function of the chlorophyll concentration, so self-shading is included. The incident irradiation is modelled using a formulation based on Skartveit and Olseth (1986, 1987). Data for global radiation are taken from the Surface Radiation Budget (Darnell *et al*. 1996). Respiration is a function of temperature only. Phytoplankton mortality is given as a constant fraction and is assumed to account also for zooplankton predation which, in this context, is included as a forcing function. Sinking rates are applied for both dead and living algae. Nitrogen and phosphorus are regenerated from the dead algae (detritus) at a constant rate.

Initial values for the nutrient fields (annual means) are interpolated from the 1×1 degree NOAA atlas (Conkright *et al*. 1994). These annual fields are also used at the open boundaries. A small, initial amount of diatoms and flagellates (2.75 $mgN \cdot m^{-3}$) is set in the model.

RESULTS AND DISCUSSION

The model was first run in the physical mode. A one-year simulation was performed. After a two-month spin-up, starting on 1 November 1989 (and assuming

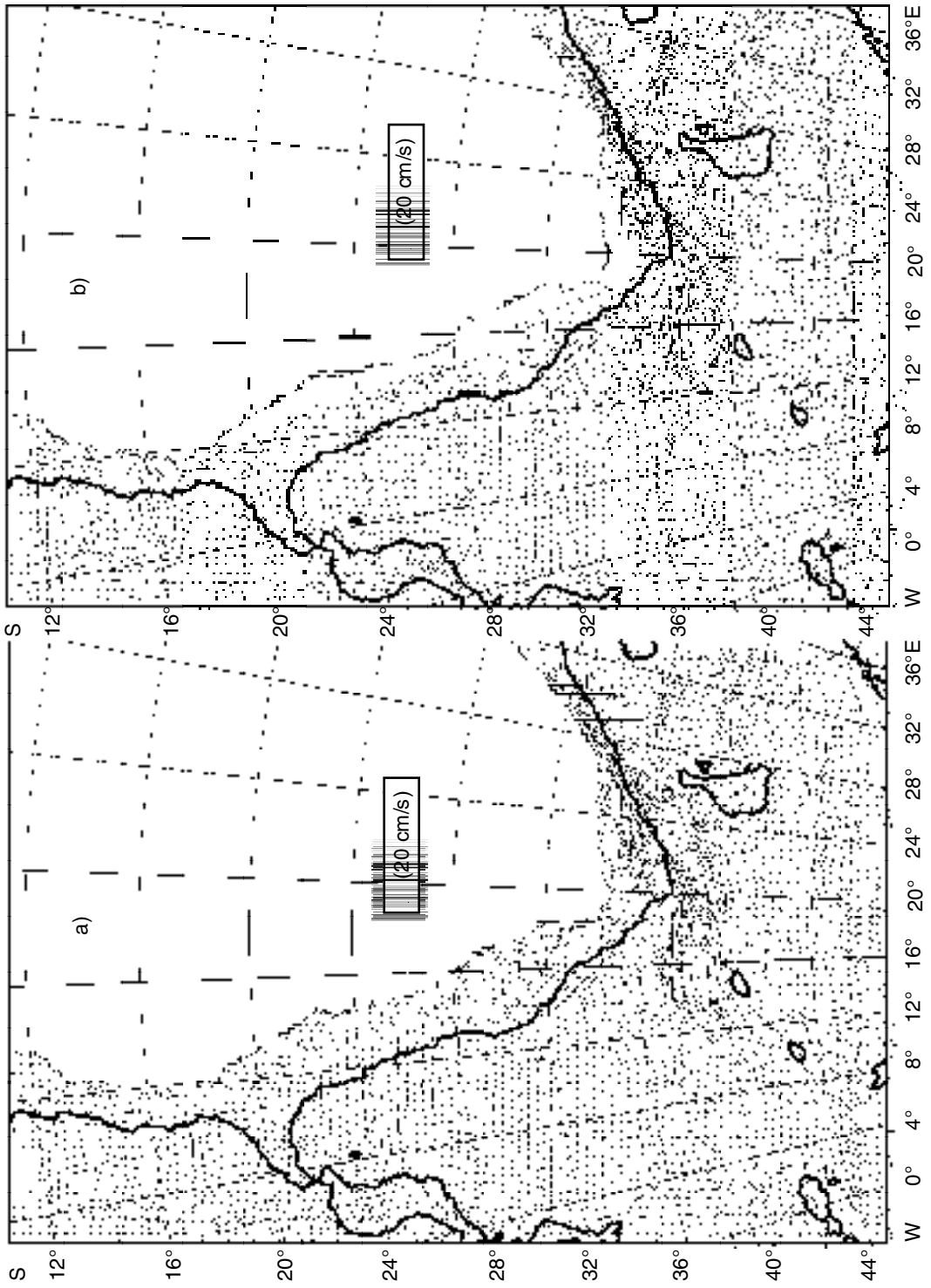

Fig. 2: Modelled annual (1990) mean velocities at (a) 10 m deep and (b) 200 m deep. The solid line is the 300-m depth contou

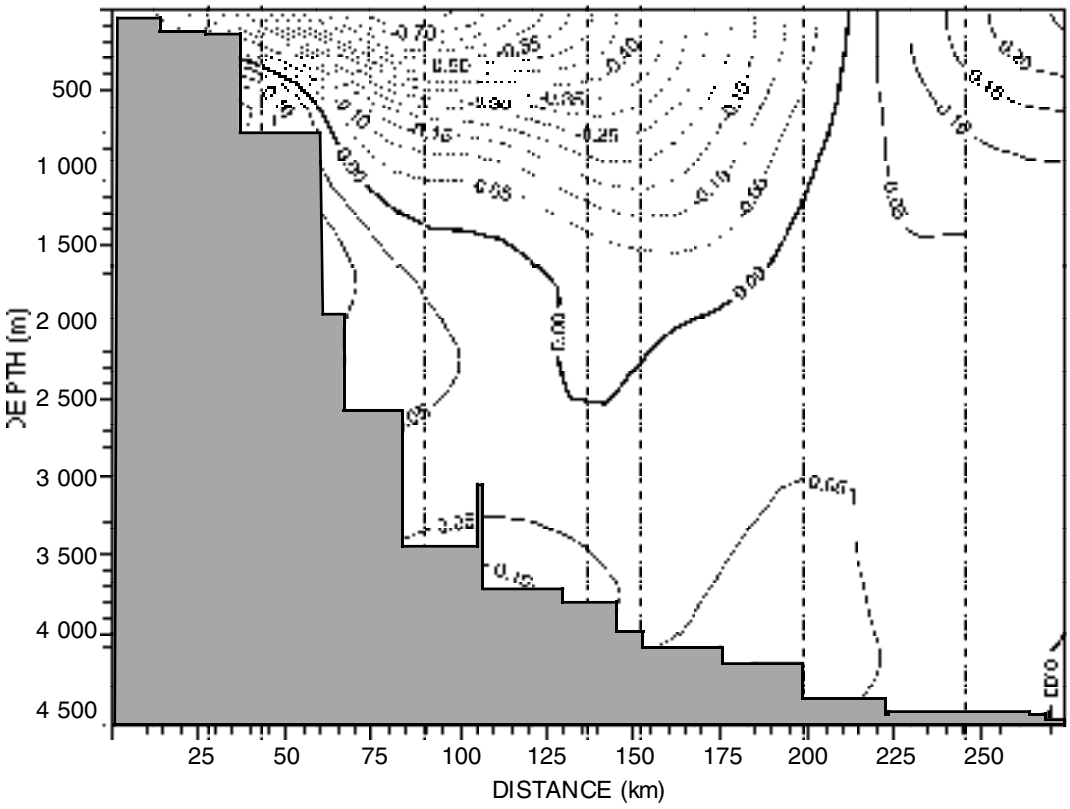

Fig. 3: Modelled annual (1990) mean velocities across the Port Elizabeth section

1990 winds valid for 1989 for this purpose) the year 1990 was simulated using the 1990 winds from the MARS archive. Results (three velocity components, salinity, temperature and water level) were stored as monthly means in the whole model domain in all sigma layers, as 25-hourly means along a section off Port Elizabeth at 26°E (Fig. 1) and as instantaneous three-dimensional fields in the whole area, three times a month (at noon on day 1, 11 and 21). Annual average fields were calculated based on the 12 monthly averages.

Circulation, temperature and salinity

Figure 2 shows the annual mean horizontal velocities at 10 and 200 m.

The Agulhas Current closes the western boundary of the South Indian Subtropical gyre. Its mean flow is composed from a component from east of Madagascar, and one from recirculation in the South-West Indian subgyre south of Madagascar, but there is also a small contribution from the Moçambique Channel (Stramma and Lutjeharms 1997). The current moves south-westwards, remaining just offshore of the continental shelf edge (Gründlingh 1983). Near Algoa Bay (26°E), it moves away from the coast as the shelf widens, develops oscillations and begins to separate from the continental shelf (Lutjeharms 1981). As the shelf edge turns northwards south of Cape Agulhas, the current continues south-westwards, leaves the shelf and turns eastwards in a large loop, the Agulhas retroflection, and becomes the Agulhas Return Current.

Coming from the north-east, the model shows a well-developed Agulhas Current that follows the east coast of South Africa. South of 27°E, it leaves the coast and closely follows the shelf-break, with a maximum annual mean velocity of more than 1.6 $m \cdot s^{-1}$ at 10 m deep. Several authors have calculated the volume transport of the Agulhas Current (see Gründlingh 1980), and the

results vary from 9 to 136 Sverdrup (1 Sv = 10^6 $m^3 \cdot s^{-1}$). Based on data from eight cruises, Gründlingh (1980) estimated a volume transport of 62 Sv in the upper 1 000 m at 31°S. Duncan (1970) found that 83% of the total flux of the Agulhas Current is transported in the upper 1 000 m. Using this relation, Gründlingh (1980) extrapolated the value to 75 ± 10 Sv over the whole water column. Stramma and Lutjeharms (1997) reported a volume transport of 65 Sv in the upper 1 000 m. The section at 31°S is too close to the model boundary, where a zero net flux was specified, even if the modelled volume transport is more than 20 Sv there. Therefore, the modelled volume transport through the Port Elizabeth section at 34°S (see Fig.1) was used instead as an approximation of the volume transport in the Agulhas Current. Through this section, the mean transport in the upper 1 500 m is estimated to be 53 Sv, and 48 Sv (91%) in the upper 1 000 m. This volume is less than half the modelled volume flux of the Agulhas Current from the FRAM model (Lutjeharms and Webb 1995).

Beal and Bryden (1997) made observations of an Agulhas undercurrent using Lowered Acoustic Doppler Current Profiler (LADCP). Stations were occupied on a 230-km section across the Agulhas Current, nominally at 32°S. The zero velocity surface from these measurements (their Fig. 3) is distinctly V-shaped, leaving the continental slope at a depth of 700 m, reaching a maximum depth of 2 500 m some 80 km offshore, before shallowing up to 1 000 m about 230 km from the coast. This is a very different vertical structure for the Agulhas Current than imposed by the traditional assumption that the zero velocity surface is generally deep and horizontal (Duncan 1970). Most notable is an undercurrent close to the continental slope, flowing north-eastwards. The core is 1 200 m deep, with velocities as large as 30 $cm \cdot s^{-1}$. Again, this section is too close to the model boundary. Therefore, the annual mean velocity for the Port Elizabeth section was used (Fig. 3). Despite the slightly different geographical location of the two sections, the model confirms the main findings from the LADCP measurements: the zero velocity surface is V-shaped, with a maximum depth of 2 500 m, and the model also gives an undercurrent flowing north-eastwards with a core close to the continental slope.

Farther downstream, the Agulhas Current departs from the shelf-break and, from the annual mean velocity fields in Figure 2, it seems to retroflect at approximately 14°E. Lutjeharms and Van Ballegooyen (1988a) found the Agulhas retroflection to occur preferentially at 20°E, with a secondary retroflection at 16°E. Occasionally (two or three times a year), retroflection occurs upstream of these positions, at about 25°E (Lutjeharms and Van Ballegooyen 1988b). From the above, the model seems to retroflect too far to the west. However, the model indicates two tangential points at about 21 and 25°E, where the opposing currents meet. This will be discussed later in the context of Agulhas Rings.

Off the Cape of Good Hope, the model produces a strong, northward flow 10 m deep, with a maximum of about 40 $cm \cdot s^{-1}$. Such a strong flow is confirmed by Boyd and Nelson (1998). This flow, the Benguela Current, bends north-westwards and separates from the coast at about 30°S. Over most of the region between 16 and 32°S, there is a north-westerly flow turning westwards offshore. This is in agreement with Stramma and Peterson (1989). Those authors estimated the northward geostrophic transport in the Benguela Current, out to 1 500 km offshore at 32°S, to be 26 Sv (σ_0 = 27.75). The same volume transport (26 Sv to 1 500 m) is also found from the annual mean modelled circulation.

The modelled annual mean current does not show onshore surface flow south of the Lüderitz upwelling cell, as has been found by several authors (Stander 1964, Boyd 1987). However, such an onshore flow is occasionally seen in the instantaneous velocity fields. Near the coast north to 20°S, with a width of only 20–50 km, the model produces a steady flow (10–15·cm^{-1}), restricted to the upper layers. This flow is probably a result of the more or less continuous upwelling winds. Farther north, the modelled nearshore currents are south-flowing, in a narrow strip. Such a poleward surface current north of Cape Frio (18°S) is also shown in the model described by Fennel (1999).

The modelled circulation pattern 200 m deep is similar to that at 10 m, but weaker. The maximum velocity in the Agulhas Current is approximately 1 $m \cdot s^{-1}$ at 200 m. However, there are three notable differences between the 200 and 10 m circulation: an anticyclonic gyre off the Angolan coast between 12 and 16°S, some topographic steering around the Walvis Ridge, and a poleward undercurrent following the shelf-break all the way from Angola to Cape Point. Such a poleward undercurrent is known to exist, and measurements from more than 150 instruments moored at depths between 40 and 600 m between Cape Point (34°30´S) and Cape Cross (21°55´S), as well as a number of ADCP profiles, have shown such a trend (Shannon and Nelson 1996). This is also confirmed in other models (Fennel 1999).

Figure 4 shows the corresponding mean salinity and temperature fields 10 m deep. Note that the FRS zone is omitted from Figure 4. It is clear that the warm and saline Agulhas Current is coming from the east, being steered by the Agulhas Bank, and being transported into the South Atlantic. Farther south, the model shows a front towards cold and fresh Subantarctic

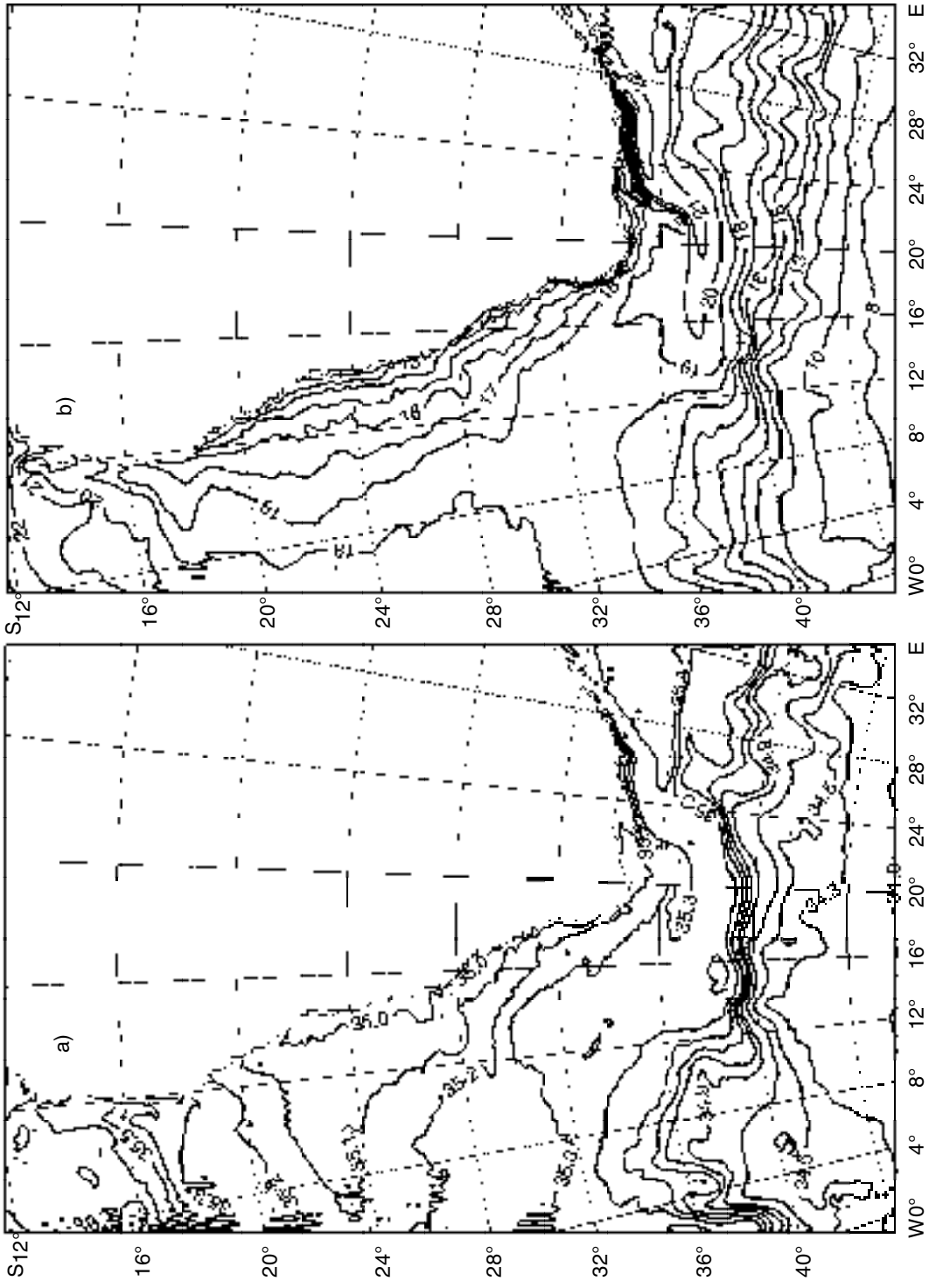

Fig. 4: Modelled (a) annual (1990) mean salinity and (b) temperature at 10 m deep. Note that the FRS zone is not included

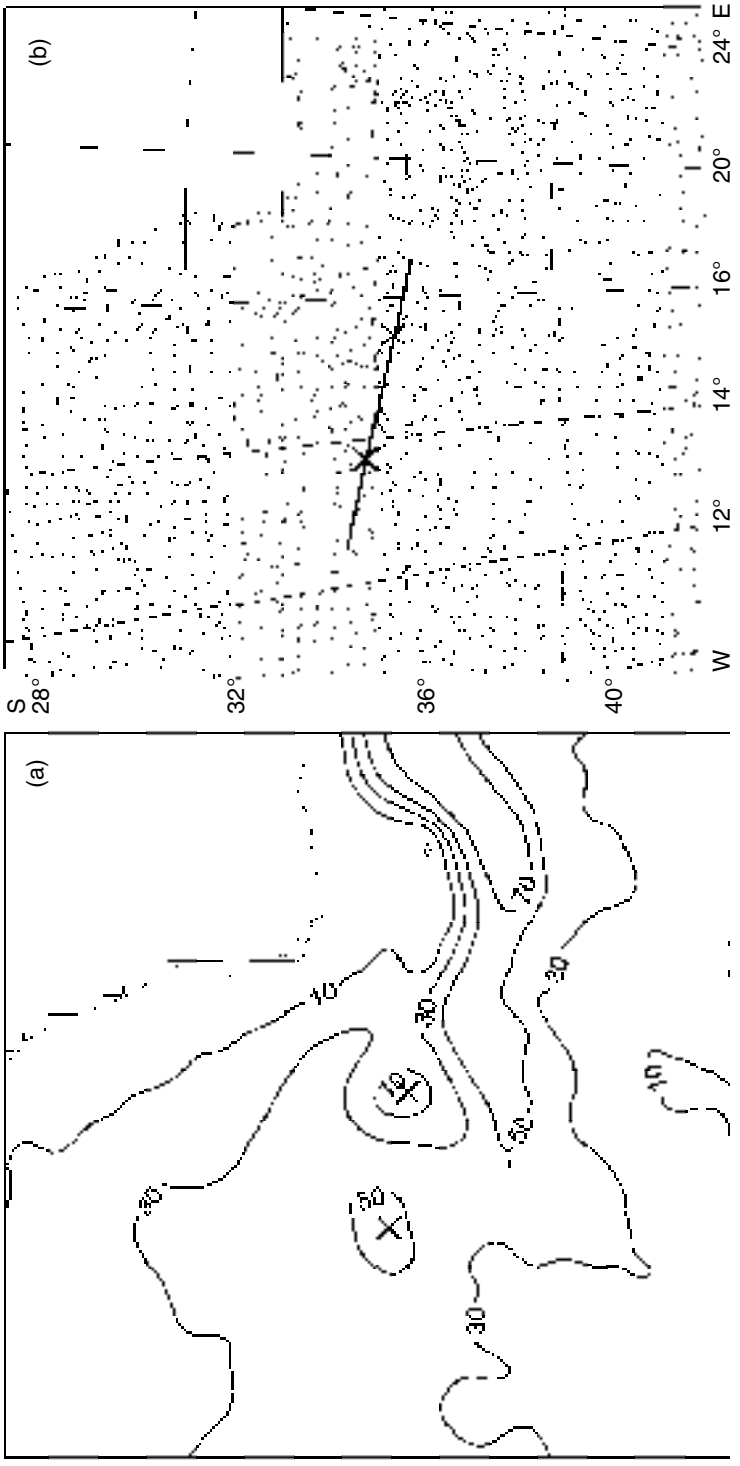

Fig. 5: Modelled (a) water level (cm) and (b) velocity field on 21 March. Note the reduced view to the lower left corner of the model domain only

water.

Over much of the area between Cape Frio (18°S) and Cape Point (34°S) there is a well-developed, longshore system of thermal fronts demarcating the seaward extent of the upwelled water. South of Lüderitz (26.5°S), a single front is usually well defined, and coincides approximately with the run of the shelf-break. Farther north, the surface manifestation of the front is more diffuse, and multiple fronts are evident on occasions (Shannon and Nelson 1996). These multiple fronts are, of course, not evident in the annual averages, but the model shows the well-developed, longshore thermal front along the coast. Also, the salinity field indicates a longshore frontal structure as far north as 18°S, but then shows clearly how the manifestation of the front changes around Lüderitz. Also in the modelled cross-shelf temperature gradient, there is a separation with an intensification south of this area. Focusing on the inner shelf (shallower than 200 m), the surface temperature difference between the inner grid point and the value at the 200-m isobath is up to 5°C south of Lüderitz, and about 3°C north of there. Investigating the nearshore temperature field, it is possible to identify several local minima that coincide with some of the well-known upwelling cells in the region. One such local minimum is found around 25–27°S and overlaps the major (geographically most extensive) upwelling cell at Lüderitz, and a second one has its centre near the Namaqua upwelling cell (30°S). Several other minima can also be identified, and they are discussed later in the context of primary production.

From seasonal distribution charts of sea surface temperature, Shannon and Agenbag (1987) showed the existence of a well-developed front intersecting the African coast between 14 and 17°S, which was also reported by Lutjeharms and Stockton (1987) and Meeuwis and Lutjeharms (1990). The front extends to a depth of at least 200 m and is particularly marked in the upper 50 m. The horizontal extent of the front is about 150–200 km from the coast, and a horizontal sea surface temperature gradient near the coast of 4°C per 1° of latitude is typical in synoptic data (Shannon *et al*. 1987). An Angola-Benguela frontal structure can also be seen from the modelled temperatures and salinities around 16–17°S. In the temperature field, it is not very intense (1°C per 1° of latitude), but the salinity field has a well-developed front. However, because the position of the front migrates seasonally, it will be weakened in an annual mean field. Investigating the vertical extent (not shown), the temperature front was found to be most dominant in the upper 30–50 m, whereas the salinity front was well developed down to at least 150 m. Similar variations were observed by Gammelsrød *et al*. (1998).

Agulhas rings

The most energetic western boundary current rings in the world's oceans are shed from the Agulhas retroflection: Agulhas Rings. As the Agulhas Current retroflects in a great anticyclonic loop, the loop can occasionally pinch off, forming a ring that is ejected into the South Atlantic Ocean (Lutjeharms and Gordon 1987). These rings are responsible for a considerable transfer of heat, salt and energy from the South Indian Ocean into the South Atlantic, and the transfer has important implications for global ocean circulation (Van Ballegooyen *et al*. 1994).

From satellite images, the spawning of Agulhas Rings seems to take place after a westward penetration of the retroflection. After an eastward jump, followed by the flow of Subantarctic or South Atlantic water into the gap, an Agulhas Ring is shed. Formation of such rings takes place on average every 39 days (Lutjeharms and Van Ballegooyen 1988a). An overview of Agulhas Rings can be found in Duncombe Rae (1991).

Originating from the warm and saline Agulhas Current, it was assumed that the rings, if they were spawned in the model, would show as clear local maxima in the instantaneous surface salinity and temperature fields. This was not the case. As a result of the small-scale noise ($2\Delta x$) in these surface fields, the rings could only be identified after a low-pass filtering procedure. However, the formation and occurrence of the rings could easily be identified from the modelled water level. In Figure 5, the modelled water level and corresponding velocity field for 21 March are given. A water level maximum to the east separates the Agulhas Current from the Agulhas Return Current. The two crosses shown in the Figure indicate a local water level maximum (the Agulhas Ring) and a minimum. The creation of such a bipole often occurs in the modelled field when a ring is spawned. Returning to the discussion concerning the retroflection of the Agulhas Current, the circulation pattern in Figure 5 suggests that a major component of the current retroflects around 19°E, in agreement with Lutjeharms and Van Ballegooyen (1988a). A large component continues westwards, before it turns northwards and forms a cyclonic and an anticyclonic eddy around the two water level extremes. Lutjeharms and Van Ballegooyen (1988a) stated that the diameter of the retroflection was fairly constant (342 ± 66 km) and comparable to the diameter of the rings. From the anticyclone around the ring, the diameter is estimated to be approximately 250 km, in agreement with measurements by Duncombe Rae (1991).

To investigate the vertical extent and structure of the Agulhas Ring, salinity and temperature profiles along an east-west section (see position in Fig. 5b) is shown

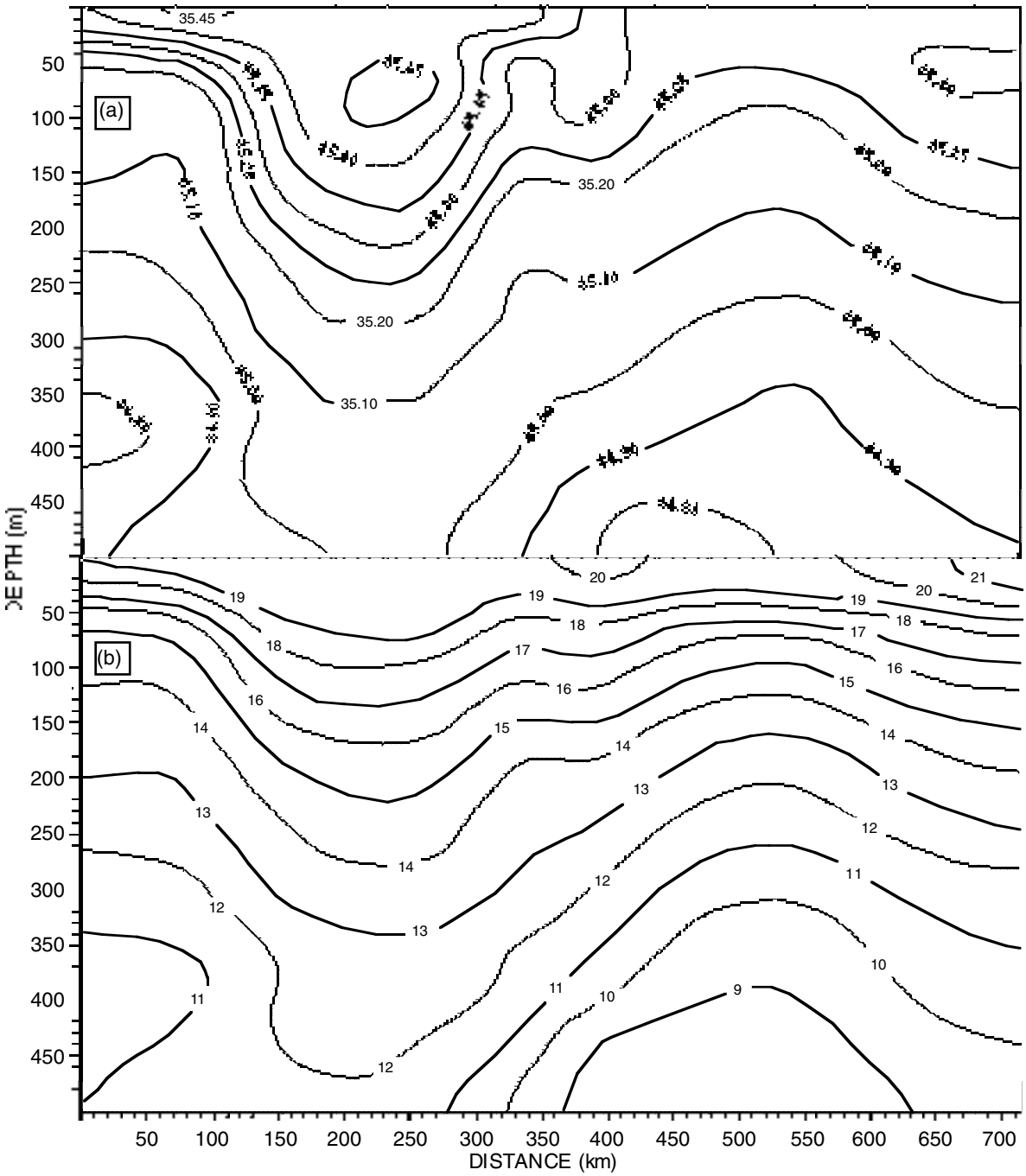

Fig. 6: Modelled (a) salinity and (b) temperature along the section shown in Figure 5b. The centre of the Agulhas Ring is at 225 km

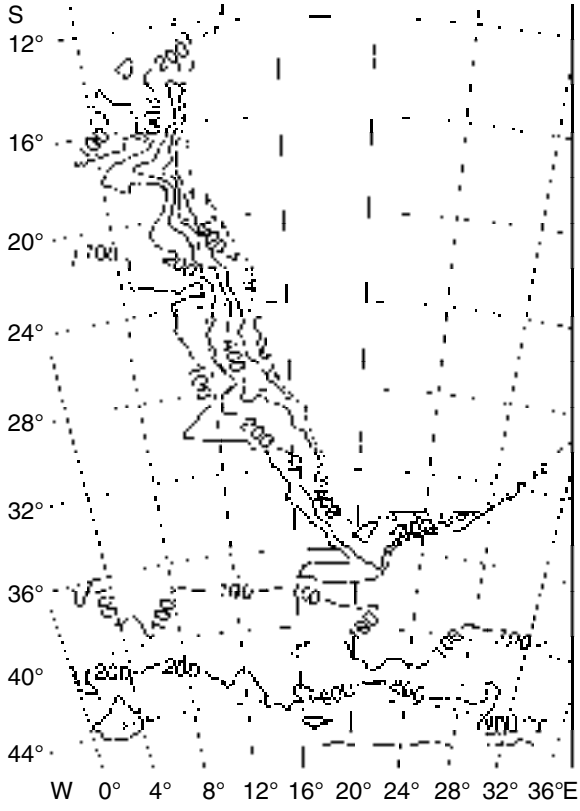

Fig. 7: Modelled depth-integrated annual (1 July 1989 – 1 July 1990) primary production ($gC \cdot m^{-2} \cdot year^{-1}$)

in Figure 6. The centre of the ring is positioned 225 km from the left endpoint, and the centre of the cyclonic feature at 520 km. From these profiles, the diameter of the ring is also close to 250 km. As mentioned earlier, the unfiltered model surface salinity and temperature fields did not show any clear signs of the Agulhas Ring. Despite this, the vertical profiles of the instantaneous fields give clear evidence of the appearance of a ring-like phenomenon. In fact, the salinity section shows a clear subsurface maximum 75 m deep, whereas the modelled temperature profile shows a deep isothermal surface layer corresponding to the ring. Duncombe Rae (1991) reported on the depth of the 10°C isotherm (h_{10}) and the difference between this isotherm at the centre and at the edge of the ring (δh_{10}), giving values for these parameters as 425–870 m (mean 645 m) and 140–510 m (mean 330 m) respectively. The corresponding values from the modelled ring are 550 and 125 m.

Agulhas Rings being shed into the South Atlantic have been tracked using satellite altimetric data. Based on tracks from seven selected eddies from GEOSAT data, Gordon and Haxby (1990) showed drift rates of 5–8 $cm \cdot s^{-1}$. Assuming the movement of the ring centre to be a typical drift rate in the model, the ring velocity is estimated to be 3 $cm \cdot s^{-1}$, by comparing the position of the water level maxima at 21 March and 1 April.

Primary production and upwelling cells

A second run was done with the coupled physical biological model system. After a 2-month spin-up, starting on 1 May 1989, the model was run for one year (1 July 1989 – 30 June 1990), again assuming that 1990 winds were also valid for 1989. Data for all prognostic variables were stored as for the physical run. In addition, the depth-integrated production ($gC \cdot m^{-2} \cdot month^{-1}$) was calculated.

In Figure 7, the depth-integrated total annual primary production ($gC \cdot m^{-2} \cdot year^{-1}$) is given. The production shows large spatial variability, with low (<100 $gC \cdot m^{-2} \cdot year^{-1}$) production in the open ocean increasing towards the coast. Along the coast there are several local maxima, and a general increase northwards, as far as the Angolan border. The absolute maximum is found near Cape Frio (Fig. 1), where the modelled annual production is about 1 400 $gC \cdot m^{-2} \cdot year^{-1}$. This is 2–3 times the production near Cape Agulhas. An increased offshore production is seen in the model results in the area just north of the Walvis Ridge, and in the extreme south. In both those areas, the initial fields also indicate higher nutrient values than in the other offshore area.

The mean production (whole model area) is 163 $gC \cdot m^{-2} \cdot month^{-1}$, of which 60% is flagellate and 40% diatom production. Horizontal maps of diatom and flagellate primary production are given in Figure 8. The production shows a clear annual cycle. The mean (whole area) production has its maximum in October and November, with approximately 23 $gC \cdot m^{-2} \cdot month^{-1}$. This is three times higher than the minimum found in May and June. The diatom and flagellate production maxima are in October and November respectively.

Using the model, it is possible to give an estimate of the total productivity in the whole Benguela system. Brown *et al.* (1991) divided the area into three (northern Benguela, southern Benguela, and South Coast), and estimated the total productivity within each area (to the 500-m depth contour) to be $75–80 \times 10^6$ tons using a production/chlorophyll *a* regression (total = 232×10^6 tons). The total production for the same area in the present model is estimated to be 218×10^6 tons.

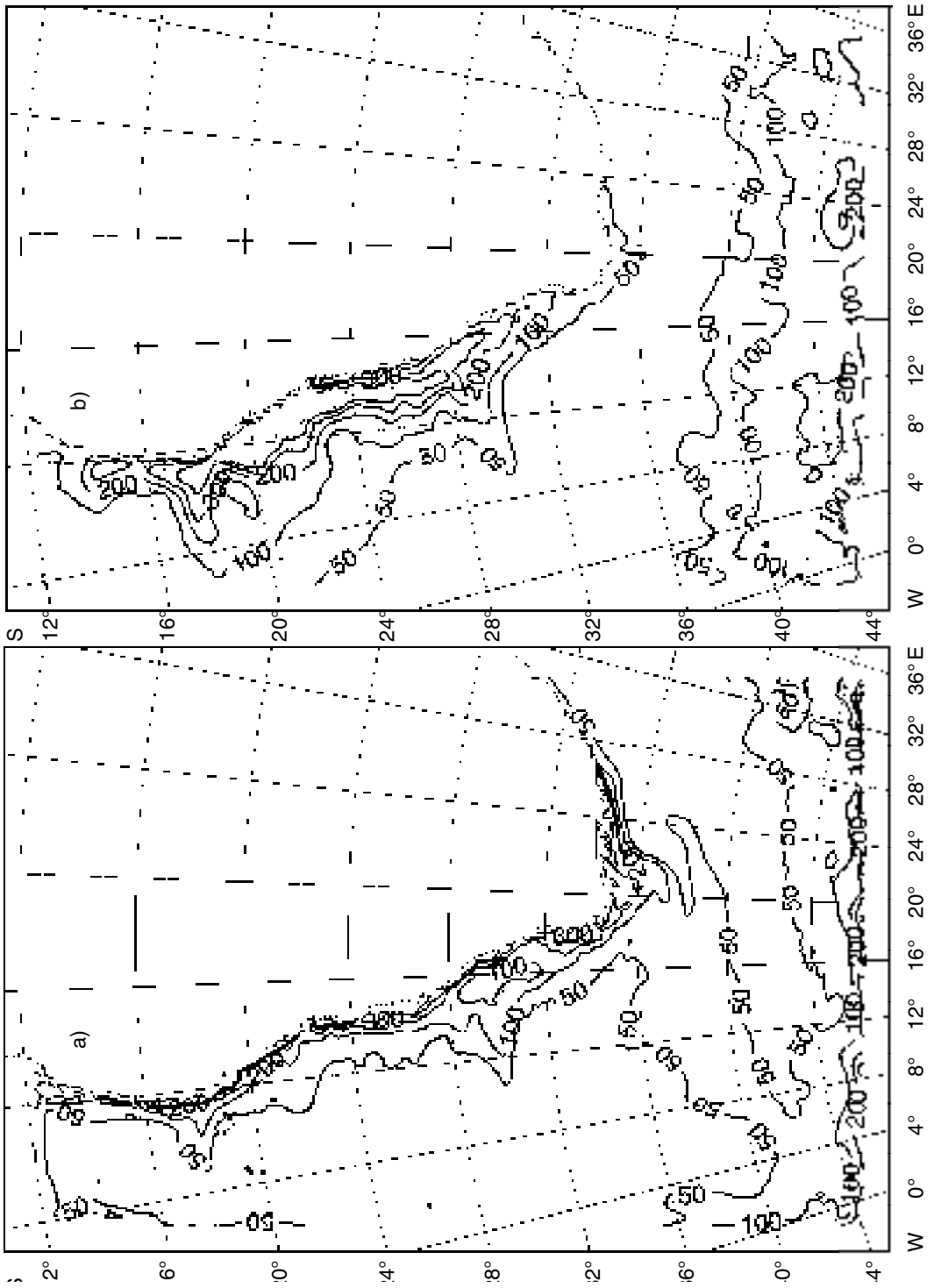

Fig. 8: Modelled depth-integrated annual (1 July 1989 – 1 July 1990) primary production ($gC \cdot m^{-2} \cdot year^{-1}$) for (a) diatoms and (b) flagellates

However, comparing values for daily production, the regression equation suggests values of 1.2, 2.0 and 1.9 $gC \cdot m^{-2} \cdot day^{-1}$ for the three areas respectively (the lowest value in the north), whereas the model proposes the highest value (1.9 $gC \cdot m^{-2} \cdot day^{-1}$) to be in the north, with only 0.85 $gC \cdot m^{-2} \cdot day^{-1}$ averaged over the southern areas. However, it should be noted that the nutrient initial and boundary fields are derived from annual means. These fields have larger concentrations of nutrients in the northern areas than in the south, and the production results would reflect these patterns.

Upwelling is a feature of the whole Benguela between Cape Frio (18°S) and Cape Point (34°S), Boyd 1987). Upwelling also extends along much of the South Coast as far as 25°E (Schumann *et al*. 1982). The wind and pressure field, topographic features and orientation of the coast result in the formation of a number of areas where upwelling is prevalent, i.e. the upwelling cells. Lutjeharms and Meeuwis (1987) distinguished eight different cells (Cunene, Namibia, Walvis Bay, Lüderitz, Namaqua, Columbine, Peninsula and the Agulhas cell), and Shannon and Nelson (1996) included three more along the South Coast (Plettenberg, St Francis and Recife). With respect to both seaward extent and sea surface temperature, Lutjeharms and Meeuwis (1987) identified the Lüderitz cell as the most intense. This cell also divides the Benguela into two regions. The cells to the south are less intense, but of fairly equal intensity, whereas the cell intensity to the north decreases equatorwards.

Focusing again on the diatom production in Figure 8, it is possible to identify several local maxima. In fact, except for the Agulhas cell, all the upwelling cells can be identified from a locally increased diatom production. The Lüderitz cell can also easily be identified as the most intense. In addition, the model suggests the northernmost cell at Cape Frio-Cunene River to be a major upwelling site, in agreement with Boyd (1987) and in keeping with the upwelling wind stress. The upwelling cells seem more distinct in the diatom production field than in the mean temperature and salinity fields in Figure 4. Upwelling transports extra nutrients to the surface layer, so the annual primary production could have an integrative function and act like an upwelling index. A more detailed picture of the upwelling on the surface temperature and salinity can be seen in instantaneous fields of these modelled parameters (not shown). In such fields, the appearance of upwelling cells, as a function of local winds and topography, are more distinct.

In contrast to the diatom production field, the upwelling maxima at the coast are not seen in the flagellate production. This can be explained from the higher affinity to light and nutrients in the diatom dynamics specified inside the model. Overlaying the two figures, it can be seen that the flagellates are more likely to produce a minimum at the location of the upwelling cells, with an increased offshore production. The explanation for such a production pattern can be found in Shannon *et al*. (1983), who showed that phytoplankton blooms occur offshore and not in the centre of active upwelling cells. This is in agreement with studies from other upwelling areas, which show that the maxima in production and biomass are found at the borders of or just outside upwelling fronts (Dengler 1985).

CONCLUDING REMARKS

In this paper a three-dimensional biophysical model for the whole Benguela upwelling system has been described. Using realistic wind forcing from 1990, two different simulations have been done. The primary task has been a validation of the model, with the focus on some of the known large-scale phenomena in the area. Based on the present set-up and forcing, the model has proven to be able to reproduce some of these main characteristics. The model shows a well-developed Agulhas Current, with surface velocities of more than 1.6 $m \cdot s^{-1}$, and a volume flux of 53 Sv, and an Agulhas Undercurrent flowing in the opposite direction. The model is also able to reproduce the Agulhas retroflection and Agulhas Rings. The volume transport of the Benguela Current is estimated to be 26 Sv, in agreement with literature estimates, and a poleward undercurrent is shown to follow the shelf-break all the way from Angola to Cape Point. From the modelled temperature and salinity fields, both the well-known longshore thermal front and the Angola-Benguela front structure can be seen. Finally, from the primary production fields, several major upwelling cells can be identified.

The present model represents a tool for gaining new insight into the complex dynamics between physics and biology in nature. However, limitations have to be taken into consideration when interpreting the results. The open boundaries are calculated from climatological seasonal fields, and the in/out flow is assuming geostrophy. The initial fields for nutrients are annual means, and the light is at present monthly means, which are assumed valid everywhere in the model domain. Clearly, the horizontal resolution is a limiting factor with respect to correct simulation of, for example, nearshore and mesoscale processes. The model does not incorporate *real* surface heat fluxes, only a relaxation towards monthly climatological sea surface temperature fields. These fields, based on seasonal climatology, are too coarse (1×1 degree) to resolve the upwelling properly, and therefore the modelled temperature

does not return to values close to its initial state near the upwelling cells after a yearly cycle.

Even if the present model has shown promising results, there is much potential for further development, including improved representation of forcing factors. Essential for all model development is validation. Proper data, also reflecting variability in time and space, are needed to fulfil this task. However, even given its limitations, the model at hand still has the potential to give additional information for some of the large-scale main scientific/management questions in the area, including the dispersion of weakly mobile organisms (fish eggs and larvae) when coupling the circulation model to a Lagrangian drifters model.

LITERATURE CITED

AKSNES, D. L., ULVESTAD, K. B., BALIÑO, B. M., BERNTSEN, J., EGGE, J. K. and E. SVENDSEN 1995 — Ecological modelling in coastal waters: towards predictive physical-chemical-biological simulation models. *Ophelia* **41**: 5–36.

BEAL, L. M. and H. L. BRYDEN 1997 — Observations of an Agulhas undercurrent. *Deep-Sea Res.* **44**: 1715–1724.

BERNTSEN, J., SVENDSEN, E. and M. OSTROWSKI 1996 — Validation and sensitivity study of a sigma-coordinate ocean model using the SKAGEX dataset. *ICES Doc.* **C.M. 1996/C:5**: 28 pp.

BLUMBERG, A. F. and G. L. MELLOR 1987 — A description of a three-dimensional coastal ocean circulation model. In *Three-Dimensional Coastal Ocean Models*. Heaps, N. S. (Ed.). Washington D. C.; American Geophysical Union: 1–16 (Coastal and Estuarine Sciences **4**).

BOUDRA, D. B. and E. P. CHASSIGNET 1988 — Dynamics of Agulhas retroflection and ring formation in a numerical model. 1. The vorticity balance. *J. phys. Oceanogr.* **18**(2): 280–303.

BOUDRA, D. B. and W. P. M. DE RUIJTER 1986 — The wind-driven circulation of the South Atlantic-Indian Ocean. 2. Experiments using a multi-layer numerical model. *Deep-Sea Res.* **33**(4A): 447–482.

BOYD, A. J. 1987 — The oceanography of the Namibian shelf. Ph.D. thesis, University of Cape Town: [xv] + 190 pp. + [i].

BOYD, A. J. and G. NELSON 1998 — Variability of the Benguela Current off the Cape Peninsula, South Africa. In *Benguela Dynamics: Impacts of Variability on Shelf-Sea Environments and their Living Resources*. Pillar, S. C., Moloney, C. L., Payne, A. I. L. and F. A. Shillington (Eds). *S. Afr. J. mar. Sci.* **19**: 27–39.

BROWN, P. C., PAINTING, S. J. and K. L. COCHRANE 1991 — Estimates of phytoplankton and bacterial biomass and production in the northern and southern Benguela ecosystems. *S. Afr. J. mar. Sci.* **11**: 537–564.

CONKRIGHT, M. E., LEVITUS, S. and T. BOYER 1994 — *World Ocean Atlas 1994. **1.** Nutrients. Tech. Rep. NOAA Atlas*. Washington D.C.; National Oceanic and Atmospheric Administration:150 pp.

COX, M. D. and K. BRYAN 1984 — A numerical model of the ventilated thermocline. *J. phys. Oceanogr.* **14**: 674–687.

DARNELL, W. L., STAYLOR, W. F., RITCHEY, N. A., GUPTA, S. K. and A. C. WILBER 1996 — Surface radiation budget: a long-term global dataset of short-wave and long-wave fluxes. http://www.agu.org/eos-elec/95206e.html.

DENGLER, A. T. 1985 — Relationship between physical and biological processes at an upwelling front off Peru, 15°S. *Deep-Sea Res.* **32**: 1301–1315.

DUNCAN, C. P. 1970 — The Agulhas Current. Ph.D. thesis, University of Hawaii: 76 pp.

DUNCOMBE RAE, C. M. 1991 — Agulhas retroflection rings in the South Atlantic Ocean: an overview. *S. Afr. J. mar. Sci.* **11**: 327–344.

GAMMELSRØD, T., BARTHOLOMAE, C. H., BOYER, D. C., FILIPE, V. L. L. and M. J. O'TOOLE 1998 — Intrusion of warm surface water along the Angolan-Namibian coast in February–March 1995: the 1995 Benguela *Niño*. In *Benguela Dynamics: Impacts of Variability on Shelf-Sea Environments and their Living Resources*. Pillar, S. C., Moloney, C. L., Payne, A. I. L. and F. A. Shillington (Eds). *S. Afr. J. mar. Sci.* **19**: 41–56.

FENNEL, W. 1999 — Theory of the Benguela upwelling system. *J. phys. Oceanogr.* **29**: 177–190.

GORDON, A. L. and W. F. HAXBY 1990 — Agulhas eddies invade the South Atlantic: evidence from Geosat altimeter and shipboard Conductivity-Temperature-Depth survey. *J. geophys. Res.* **95**(C3): 3117–3125.

GRÜNDLINGH, M. L. 1980 — On the volume transport of the Agulhas Current. *Deep-Sea Res.* **27**(7A): 557–563.

GRÜNDLINGH, M. A. 1983 — On the course of the Agulhas Current. *S. Afr. geogrl J.* **65**: 49–57.

HOLLAND, W. R., ZLOTNICKI, V. and L-L. FU 1991 — Modelled time-dependent flow in the Agulhas retroflection region as deduced from altimeter data assimilation. *S. Afr. J. mar. Sci.* **10**: 407–427.

IOC, IHO and BODC 1994 — The general bathymetric chart of the oceans (GEBCO) digital atlas. http://www.nbi.ac.uk/bodc/gebco.html.

LEVITUS, S. and T. BOYER 1994 — *World Ocean Atlas 1994. **4**. Temperature. Tech. Rept. NOAA Atlas*. Washington D.C.; National Oceanic and Atmospheric Administration: 117 pp.

LEVITUS, S., BURGETT, R. and T. BOYER 1994 — *World Ocean Atlas 1994. **3**. Salinity. Tech. Rept. NOAA Atlas*. Washington D.C.; National Oceanic and Atmospheric Administration: 99 pp.

LUTJEHARMS, J. R. E. 1981 — Features of the southern Agulhas Current circulation from satellite remote sensing. *S. Afr. J. Sci.* **77**(5): 231–236.

LUTJEHARMS, J. R. E. and A. L. GORDON 1987 — Shedding of an Agulhas Ring observed at sea. *Nature, Lond.* **325**(7000): 138–140.

LUTJEHARMS, J. R. E. and J. M. MEEUWIS 1987 — The extent and variability of South-East Atlantic upwelling. In *The Benguela and Comparable Ecosystems*. Payne, A. I. L., Gulland, J. A. and K. H. Brink (Eds). *S. Afr. J. mar. Sci.* **5**: 51–62.

LUTJEHARMS, J. R. E. and P. L. STOCKTON 1987 — Kinematics of the upwelling front off southern Africa. In *The Benguela and Comparable Ecosystems*. Payne, A. I. L., Gulland, J. A. and K. H. Brink (Eds). *S. Afr. J. mar. Sci.* **5**: 35–49.

LUTJEHARMS, J. R. E. and R. C. VAN BALLEGOOYEN 1988 — Anomalous upstream retroflection in the Agulhas Current. *Science, N.Y.* **240**: 1770–1772.

LUTJEHARMS, J. R. E. and R. C. VAN BALLEGOOYEN 1988 — The retroflection of the Agulhas Current. *J. phys. Oceanogr.* **18**(11): 1570–1583.

LUTJEHARMS, J. R. E. and D. J. WEBB 1995 — Modelling the Agulhas Current system with FRAM (Fine Resolution Antarctic Model). *Deep-Sea Res.* **42**(4): 523–551.

LUTJEHARMS, J. R. E., WEBB, D. J. and B. A. DE CUEVAS 1991 — Applying the Fine Resolution Antarctic Model

(FRAM) to the ocean circulation around southern Africa. *S. Afr. J. Sci*. **87**(8): 346–349.
LUTJEHARMS, J. R. E., WEBB, D. J., DE CUEVAS, B. A. and S. R. THOMPSON 1995 — Large-scale modelling of the South-East Atlantic upwelling system. *S. Afr. J. mar. Sci*. **16**: 205–225.
MARTINSEN, E. A. and H. ENGEDAHL 1987 — Implementation and testing of a lateral boundary scheme as an open boundary condition in a barotropic ocean model. *Coast. Engng* **11**: 603–627.
MEEUWIS, J. M. and J. R. E. LUTJEHARMS 1990 — Surface thermal characteristics of the Angola-Benguela front. *S. Afr. J. mar. Sci*. **9**: 261–279.
MELLOR, G. L. and T. YAMADA 1982 — Development of a turbulence closure model for geophysical fluid problems. *Revs Geophys. Space Phys*. **20**: 851–875.
MESINGER, F. and A. ARAKAWA 1976 — *Numerical Methods Used in Atmospheric Models*. Global Atmospheric Research Programme. Series 17: 64 pp.
OEY, L-Y. and P. CHEN 1992 — A model simulation of circulation in the north-east Atlantic shelves and seas. *J. geophys. Res*. **97**(C12): 20087–20115.
SARMIENTO, J. L. and K. BRYAN 1982 — An ocean transport model for the North Atlantic. *J. geophys. Res*. **87**(C1): 394–408.
SCHUMANN, E. H., PERRINS, L-A. and I. T. HUNTER 1982 — Upwelling along the south coast of the Cape Province, South Africa. *S. Afr. J. Sci*. **78**(6): 238–242.
SHANNON, L. V. and J. J. AGENBAG 1987 — Some aspects of the physical oceanography of the boundary zone between the Benguela and Angola Current systems. *Colln scient. Pap. int. Commn SE. Atl. Fish*. **14**(2): 249–261.
SHANNON, L. V. and G. NELSON 1996 — The Benguela: large scale features and processes and system variability. In *The South Atlantic: Present and Past Circulation*. Wefer, G., Berger, W. H., Siedler, G. and D. J. Webb (Eds). Berlin; Springer: 163–210.
SHANNON, L. V., AGENBAG, J. J. and M. E. L. BUYS 1987 — Large and mesoscale features of the Angola-Benguela front. In *The Benguela and Comparable Ecosystems*. Payne, A. I. L., Gulland, J. A. and K. H. Brink (Eds). *S. Afr. J. mar. Sci*. **5**: 11–34.
SHANNON, L. V., MOSTERT, S. A., WALTERS, N. M. and F. P. ANDERSON 1983 — Chlorophyll concentrations in the southern Benguela Current region as determined by satellite (*Nimbus-7* coastal zone colour scanner). *J. Plankt. Res*. **5**(4): 565–583.
SKARTVEIT, A. and J. A. OLSETH 1986 — Modelling slope irradiance at high latitudes. *Solar Energy* **36**: 333–344.
SKARTVEIT, A. and J. A. OLSETH 1987 — A model for the diffuse fraction of hourly global radiation. *Solar Energy* **37**: 271–274.
SKOGEN, M. D. 1993 — *A User's Guide to NORWECOM, the NORWegian ECOLogical Model System. Tech. Rep.Inst. Mar. Res., Bergen* **6**: 23 pp.
SKOGEN, M. D., SVENDSEN, E., BERNTSEN, J., AKSNES, D. and K. B. ULVESTAD 1995 — Modelling the primary production in the North Sea using a coupled three-dimensional physical-chemical-biological ocean model. *Estuar. coast. Shelf Sci*. **41**: 545–565.
SKOGEN, M. D., SVENDSEN, E. and M. OSTROWSKI 1997 — Quantifying volume transports during SKAGEX with the Norwegian Ecological Model system. *Continent. Shelf Res.* **17**: 1817–1837.
STANDER, G. H. 1964 — The Benguela Current off South West Africa. *Investl Rep. mar. Res. Lab. S.W. Afr*. **12**: 43 pp. + Plates 5–81.
STRAMMA, L. and J. R. E. LUTJEHARMS 1997 — The flow field of the subtropical gyre of the South Indian Ocean. *J. geophys. Res*. **102**(C3): 5513–5530.
STRAMMA, L. and R.G. PETERSON 1989 — Geostrophic transport in the Benguela Current region. *J. phys Oceonogr*. **19**: 1440–1448.
SVENDSEN, E., FOSSUM, P., SKOGEN, M. D., ERIKSRØD, G., BJØRKE, H., NEDRAAS, K. and A. JOHANNESSEN 1995 — Variability of the drift patterns of spring spawned herring larvae, and the transport of water along the Norwegian shelf. *ICES Doc.* **C. M. 1995/Q:25**: 29 pp.
SVENDSEN, E., BERNTSEN, J., SKOGEN, M. D., ÅDLANDSVIK, B. and E. MARTINSEN 1996 — Model simulation of the Skagerrak circulation and hydrography during SKAGEX. *J. mar. Syst*. **8**: 219–236.
THE FRAM GROUP 1991 — An eddy resolving model of the Southern Ocean. *Trans. Am. geophys. Un*. **72**(15): 169, 174–175.
VAN BALLEGOOYEN, R. C., GRÜNDLINGH, M. L. and J. R. E. LUTJEHARMS 1994 — Eddy fluxes of heat and salt from the southwest Indian Ocean into the southeast Atlantic Ocean: a case study. *J. geophys. Res*. **99**(C7): 14053–14070.
VAN FOREEST, D. and G. B. BRUNDRIT 1982 — A two-mode numerical model with applications to coastal upwelling. *Prog. Oceanogr*. **11**: 329–392.